AIAA JOURNAL
Vol. 49, No. 7, July 2011

Adaptive Control in an Axial Turbofan: Model-Free Implementation with Short Response Time

Olaf Wiederhold,* Rudibert King,† and Bernd R. Noack‡
Berlin Institute of Technology, 10623 Berlin, Germany
Lars Neuhaus,§ Wolfgang Neise,¶ and Lars Enghardt**
DLR, German Aerospace Center, 10623 Berlin, Germany
and
Marius Swoboda††
Rolls-Royce Deutschland, Ltd. & Co. KG, 15827 Dahlewitz, Germany

DOI: 10.2514/1.J050702

An adaptive control strategy is implemented in a single-input/single-output experiment to improve the aerodynamic performance of an axial turbofan. Pulsed blowing into the blade tip region is used to prevent flow separation. A slope-seeking control approach is shown to be able to extend the operating region of the engine without an explicit process model. By this, flow separation can be mitigated for smaller flow coefficients. The proposed closed-loop control strategy is capable of both driving the system back to stable operating conditions automatically and stabilizing operation in the presence of large-amplitude disturbances. Moreover, it is possible to accelerate the closed-loop control performance by one order of magnitude, compared with classical extremum-seeking control. By this, an extended Kalman filter is applied that enables a rapid determination of gradients of the corresponding characteristic diagram.

Nomenclature

A	=	cross-sectional area, m^2
a	=	amplitude of perturbation
c	=	blade chord length, mm
D	=	impeller diameter, mm
f_{act}	=	actuation frequency, Hz
f'_{ref}	=	reference slope
$\hat{f}'$	=	estimated gradient
G_{BP}	=	transfer function of a bandpass filter
G_{LP}	=	transfer function of a low-pass filter
k	=	gain
$\dot{m}_{act}$	=	actuator mass flow, kg/s
m_{in}	=	injected mass flow, kg/s
$\dot{m}_{rot}$	=	total rotor mass flow, kg/s
n	=	rotary speed, rpm
P_{el}	=	electric power input to drive motor, W
P_{inj}	=	aerodynamic power of injected air flow, W
P_{motor}	=	power of drive motor, W
Q	=	volume flow of the fan, m^3/s
s	=	tip clearance, mm
U	=	impeller tip speed, m/s
$u(t)$	=	control input
u_{inj}	=	speed of injected air at the outlet of the nozzle, m/s
$y(t)$	=	controlled process variable
Δp_{tot}	=	total fan pressure, Pa
Δt	=	time step, s
ε	=	hub-to-tip ratio
ζ	=	nondimensional tip clearance
ζ_{RS}	=	normalized rotor stator distance
η	=	approximate total fan efficiency
η_{el}	=	efficiency of the drive motor at $n = 3000$ rpm
θ	=	blade stagger angle
ρ	=	air density, kg/m^3
ϕ	=	flow coefficient
ψ	=	pressure coefficient
ω_{BP}	=	cutoff frequency of high-pass filter, Hz
ω_{LP}	=	cutoff frequency of low-pass filter, Hz
ω_{sin}	=	perturbation frequency, Hz

Presented as Paper 2009-4175 at the AIAA Fluid Dynamic Conference, San Antonio, TX, 22–26 June 2009; received 29 July 2010; revision received 11 February 2011; accepted for publication 22 February 2011.

*Research Engineer, Institute of Plant Technology, Chair of Measurement and Control.

†Professor, Institute of Plant Technology, Chair of Measurement and Control, Hardenbergstrasse 36a. Member AIAA.

‡Director of Research CNRS, Institut P′, CNRS, Université de Poitiers, ENSMA, UPR 3346, Département Fluides, Thermique, Combustion, CEAT, 43 rue de l'Aérodrome, F-86036 Poitiers Cedex, France.

§Research Engineer, Institute of Propulsion Technology, Department of Engine Acoustics.

¶Professor, Institute of Propulsion Technology, Department of Engine Acoustics.

**Professor, Institute of Propulsion Technology, Department of Engine Acoustics, Müller-Breslau-Strasse 8.

††Senior Research Engineer, Design Systems Engineering, Eschenweg 11, Blankenfelde-Mahlow.

I. Introduction

MODERN turbomachine technology has to satisfy high standards concerning noise and pollution requirements as well as efficiency demands. Active flow control (AFC) offers an enormous optimization potential [1] to meet these demands by mitigating noise [2,3] or by damping instabilities [4–6]. Within a turbomachine in an aircraft propulsion system, stable operating conditions have to be guaranteed and instabilities have to be avoided. This requirement limits the efficiency, as the engines have to be operated at a safe distance from the stall line (see, e.g., Walsh and Fletcher [7] or Tavakoli et al. [8]).

Controlling flow phenomena actively shows significant advantages compared with passive means. Although geometric modifications such as vortex generators [9] and guide vanes are irremovable, an active control system is capable of avoiding unnecessary interference when control is dispensable. Moreover, AFC is able to react to changes in the operating conditions and/or the occurrence of sudden disturbances by appropriately adapting the actuation

amplitudes and phase angles [10]. In this regard, closed-loop concepts are substantially better suited than open-loop methods [11].

The present paper is concerned with extremum-seeking closed-loop control approaches [12–14], which are applied to stabilize the stalled flowfield of an axial fan by suppressing flow separation. By this, the usable aerodynamic range is increased. Pulsed blowing into the blade tip region is used in order to inhibit the secondary flowfield over the tips of the rotor blades, which is caused by the static pressure difference between the suction and pressure sides (see Neuhaus and Neise [3] or Inoue and Kuroumaru [15]). The tip clearance flow is important for the aerodynamic performance of the fan as it causes the main flow to evade toward the hub and thus the blade's stall (see Kameier and Neise [9]). However, the exact physics still remains widely unknown [9]. Through air injection in the blade tip region, the secondary flow can be reduced and by that the effective cross-sectional area for the fluid to flow increases again (see Neuhaus and Neise [3]). Alternatively, a number of authors also report the successful application of air injection upstream of the fan rotor to mitigate rotating stall and compressor surge [16,17].

Especially regarding complex technical setups, the presented control methods in this contribution provide an attractive alternative to classical model-based closed-loop control approaches, as they are used, for example, in Nelson et al. [18] or Weigl et al. [16], because the derivation of a process model is not necessary.

The proposed extremum-seeking control method has already been used in turbomachinery by Lemke et al. [19] to reduce noise from secondary noise sources significantly. Wang et al. [20] apply the control approach to inhibit surge via bleed valves. However, the experiments show a quite slow control performance. Within this investigation, it can be shown that a refined version of an extremum-seeking controller [21] is capable of accelerating the control performance considerably by exploiting an extended Kalman filter (EKF) [22] approach. Finally, the robustness of the controllers proposed is tested by introducing large-amplitude disturbances to the system.

The paper is organized as follows: The experimental setup is reviewed in Sec. II, followed by extremum-seeking control and its extensions in Sec. III. The controller results are presented in Sec. IV. The paper closes with conclusions and an outlook in Sec. V.

II. Experimental Setup

A. Test Rig

The closed-loop control experiments are conducted at a low-speed axial fan with outlet guide vanes. The same test rig is also used by Neuhaus and Neise [3] and Kameier and Neise [9] for fan noise investigations.

Figure 1 shows the experimental setup with its major dimensions. The principal features of the fan stage are listed in Table 1.

Table 1 Principal dimensions of the fan stage

Impeller diameter D, mm	452.4
Hub-to-tip ratio ε	0.62
Blade profile	NACA 65
Blade number Z	24
Number of stator vanes V	16
Axial distance rotor/stator ζ_{RS}	1.3
Blade chord length at tip, mm	43
Max. blade thickness at tip, mm	3
Tip clearance gap, mm	0.6
Design speed n, rpm	3000
Blade stagger angle at tip, °	27
Rotor mass flow at $\phi = 0.3$, kg/s	4.6

B. Actuation

Air injection is realized by 24 slit nozzles that are mounted flush with the inner casing wall and uniformly distributed over the circumference of the casing, as shown in Fig. 2. By that, the flowfield at the tip clearance gap can be influenced. The angle between the jet axis and the interior casing wall is 15°. The axial position of the air injection slit is $\xi = x/c = 16.6\%$ downstream of the leading edge of the rotor blades. This is where the profile thickness is maximal. In earlier investigations, Neuhaus and Neise [23] found this axial position to be the most effective in respect to the needed injected mass flow.

As preliminary experiments showed that valves with a high actuation frequency and a large mass flow rate at the same time are not available until now, the present publication focuses on an actuation concept with a low and fixed frequency. The used valves (Festo, Inc., type MPYE-5) have a frequency range of 0 to 200 Hz. To adjust the injected mass flow, the duty cycle can be varied from 0 to 100% (completely closed to fully open).

In preceding experiments, no actuation frequency within the usable range of 0 to 200 Hz was found that has a peculiar strong effect on the flow. Therefore, an actuation frequency of $f_{act} = 60$ Hz is adjusted. This choice provides a compromise between the desired flow control authority and the unwanted noise production.

For the generation of the control signal in real-time a digital signal processor (DSP) (dSpace controller board DS 1005, A/D converter board DS 2003, D/A converter board DS 2103) is used.

C. Fan Characteristics

To evaluate the effect of the air injection on the aerodynamic fan performance, the pressure coefficient ψ and the efficiency η are determined as a function of the flow coefficient ϕ. The fan static pressure rise is measured with conventional static pressure taps in the inlet nozzle and in the outlet duct; in both cases, four taps are uniformly distributed over the circumference. Since the inner diameters of the inlet nozzle and outlet duct are the same (500 mm), the fan static pressure rise equates the fan total pressure Δp_{tot}. The fan pressure coefficient ψ is defined as

$$\psi = \frac{\Delta p_{tot}}{\rho U^2/2} \tag{1}$$

with air density ρ and rotor blade tip speed U. The approximated total fan efficiency is determined with the power of the drive motor $P_{motor} = \eta_{el} P_{el}$ plus the power of the injected air jets P_{inj},

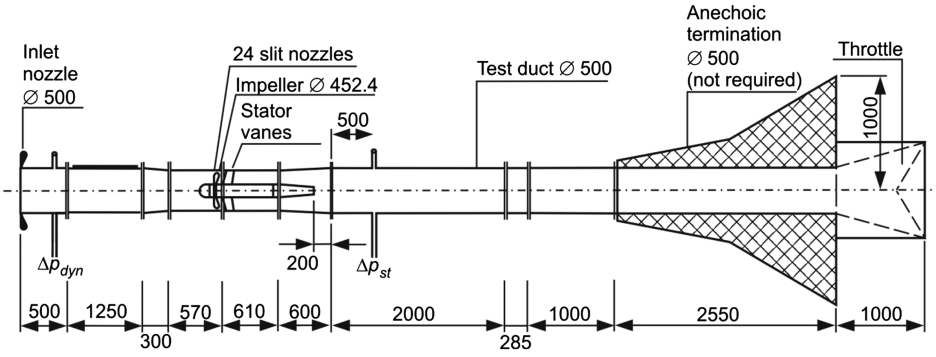

Fig. 1 Experimental setup (dimensions in millimeters).

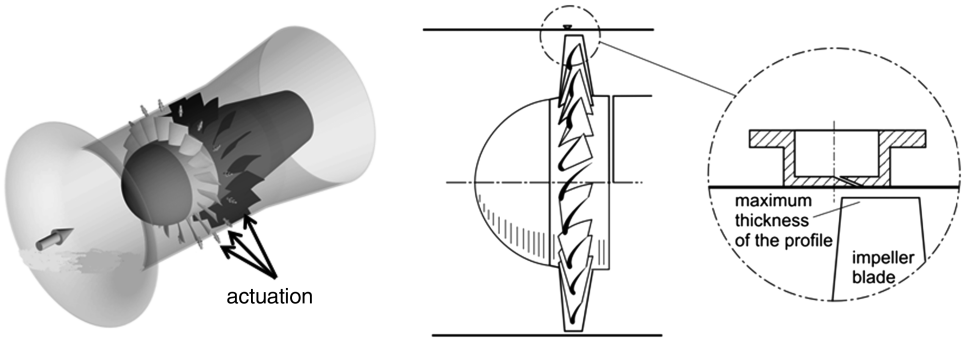

Fig. 2 Position of the actuation and schematic view of a slit nozzle.

$$\eta = \frac{\Delta p_{\text{tot}} Q}{P_{\text{motor}} + P_{\text{inj}}} \tag{2}$$

with the volume flow Q of the fan. P_{inj} is defined by the injected amount of air and the injection pressure by $P_{\text{inj}} = \dot{m}_{\text{act}} u_{\text{inj}}^2$. The flow coefficient is the normalized flow rate of the fan:

$$\phi = \frac{Q}{\pi (D/2)^2 U} \tag{3}$$

By moving the throttle, the volume flow Q of the fan is changed and the operating point of the system is shifted. In the closed-loop control experiments, this mechanism is used to simulate disturbances acting on the system.

Figure 3 shows the pressure coefficient and efficiency for the baseline case, with steady and with pulsed air injection (f_{act}= 60 Hz, duty cycle 50%). To make both actuated cases comparable, the injected mass flow is held constant. A proportional–integral–derivative controller is used to adapt the opening amplitude of the proportional directional valves in such a way that an injected mass flow of $m_{\text{in}} = \dot{m}_{\text{act}}/\dot{m}_{\text{rot}} = 1.1\%$ (Bronkhorst F-203AC-FBB-00-V, accuracy $\pm 1\%$) is provided in each case. The injected actuator mass flow $\dot{m}_{\text{act}}$ is referred to the total mass flow of the rotor with a completely open throttle $\dot{m}_{\text{rot}}(\phi = 0.3) = 4.6$ kg/s.

When the flow coefficient is decreased, the pressure coefficient and the efficiency rise until the operating point with maximum efficiency is reached. In the case without flow control, the characteristic parameters at this point are $\phi = 0.23$, $\psi = 0.41$, and $\eta = 0.86$. After that, the pressure coefficient continues to rise, whereas the efficiency is diminished until the stall point is reached at $\phi = 0.173$, $\psi = 0.46$, and $\eta = 0.79$. Further decreasing of ϕ leads to flow separation in the baseline case (no actuation), which is indicated by the drop of the pressure coefficient and a steeper decline in the efficiency curve. In contrast to that, in both cases with actuation, the pressure coefficient can be held at a level of $\psi = 0.46$, and the stall point is shifted toward lower values of the flow coefficient. The largest range of stable operating conditions is observed with steady air injection. With the presented setup and with 60 Hz actuation, 20 blades pass the actuation location. If an actuation frequency larger than the blade-passing frequency would be possible, we speculate that AFC might benefit from a synchronized actuation with respect to the actual position of an individual blade.

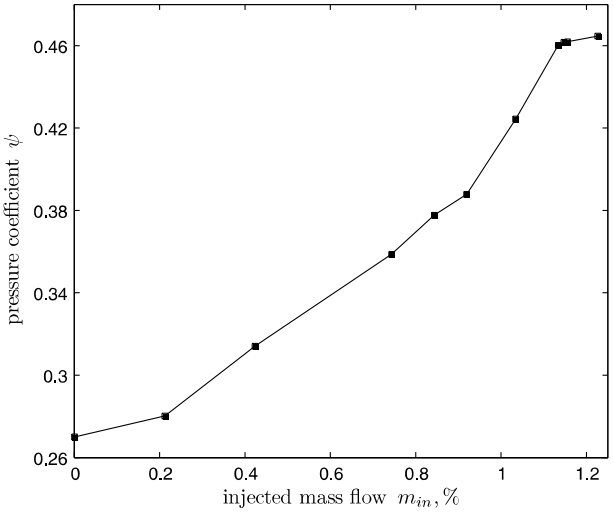

Fig. 4 Steady-state map $\psi = f(m_{\text{in}})$, with $m_{\text{in}} = \dot{m}_{\text{act}}/\dot{m}_{\text{Rot}}$.

D. Steady-State Map

Closed-loop control experiments are conducted at a fixed throttle position of the test facility within the stalled operating range. The

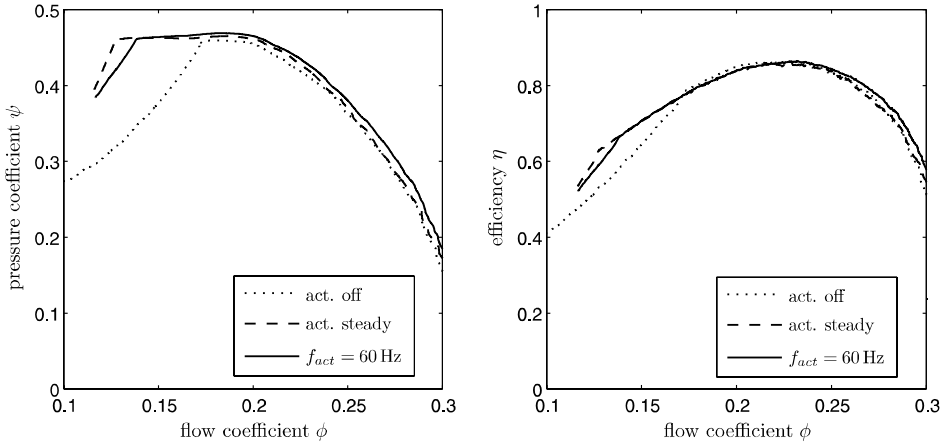

a) b)

Fig. 3 Plots of a) pressure coefficient and b) efficiency as functions of the flow coefficient for steady, pulsed, and no air injection; $n = 3000$ rpm, injected mass flow $m_{\text{in}} = 1.1\%$.

relation between the injected mass flow of the nozzles m_{in} and the corresponding values of the pressure rise ψ can be seen in Fig. 4 as a steady-state map. The injected mass flow is chosen as control input $u(t) = m_{in}$, and the controlled process variable is the pressure coefficient $y(t) = \psi$. Without actuation $[u(t) = m_{in} = 0]$, the corresponding flow coefficient is $\phi = 0.11$. At this operating point, pressure coefficient values of $\psi < 0.46$ are an indicator of stalled flow conditions. To reattach the flow, an injected mass flow of about $m_{in} = 1.17\%$ is necessary. This cannot only be observed in Fig. 4, but is clearly audible during the experiments. The reattachment point is exactly detectable at this ψ value with a microphone. This steady-state map also shows a slight increase in ψ for $m_{in} > 1.17\%$, although the flow is assumed to be essentially attached. As detailed flow visualizations inside the fan are not possible, the reason for this further increase is not clear. This small gradient will cause an overshoot of the actuation for the classical extremum-seeking control, however, as shown below.

III. Control

The slope-seeking control and as a special case the extremum-seeking control algorithms proposed are adaptive gradient-based, model-independent feedback schemes. They are capable of finding optimal actuation parameters [14,19,21]. The interest in extremum-seeking control applications rose substantially when the stability could be proven by Krstic and Wang [13], although the basic idea was already proposed long ago (cf. Morosanov [24] from 1957). When designing a controller, the challenge usually is to find a compromise between the effort of controller synthesis and control speed. In model-based control, the major part of the whole controller layout process is often spent finding a validated model, repeating model identification a few times (see Fig. 5). The benefit of a model-based synthesis is its superior bandwidth, i.e., a fast system response. In contrast, extremum-seeking control as a variant of adaptive control is applicable immediately and only needs to be tuned afterward. This is a great advantage; however, the approach suffers from a slow control performance. In this paper we start with a classical extremum-seeking controller. The initially slow control speed is then gradually increased by inclusion of extensions.

A. Slope-Seeking Controller

As extremum-seeking control is the simpler variant of the general slope-seeking control, the former is reviewed first. Extremum-seeking control is a suitable method for the control of nonlinear plants characterized by an output extremum in the steady-state map [13,21]. The control approach functions without a model of the plant to be controlled.

The basic single-input/single-output extremum-seeking closed-control loop is illustrated in the block diagram in Fig. 6 for the case of maximization. The process to be controlled is presented by both its steady-state map $y_s = f(u_s)$ and its dynamical model, to facilitate further discussion.

To drive the output of the plant to the maximal steady-state value, $y_s = y_s^*$ the average value u_s of the control input is $u(t)$ optimized online. In this manner, extremum-seeking control functions without knowing the steady-state input–output map $y_s = f(u_s)$. The controller works as follows (see also Fig. 6). The initial control input u_0, which is calculated by some higher level control hierarchy or set to zero, is superimposed with a sinusoidal signal $a\sin(\omega_{sin}t)$ with a small amplitude a and a term $\Delta u(t)$ described below:

$$u(t) = u_0 + a\sin(\omega_{sin}t) + \Delta u(t) \tag{4}$$

If the dynamics of the process are fast compared with the harmonic perturbation, the output of the process will also be approximately sinusoidal, initially centered around $y_{s,0} = f(u_0)$. The amplitude will be determined by the unknown gradient f, i.e., af'. Hence, in general, the output will read

$$y(t) \approx y_s + af'\sin(\omega_{sin}t) \tag{5}$$

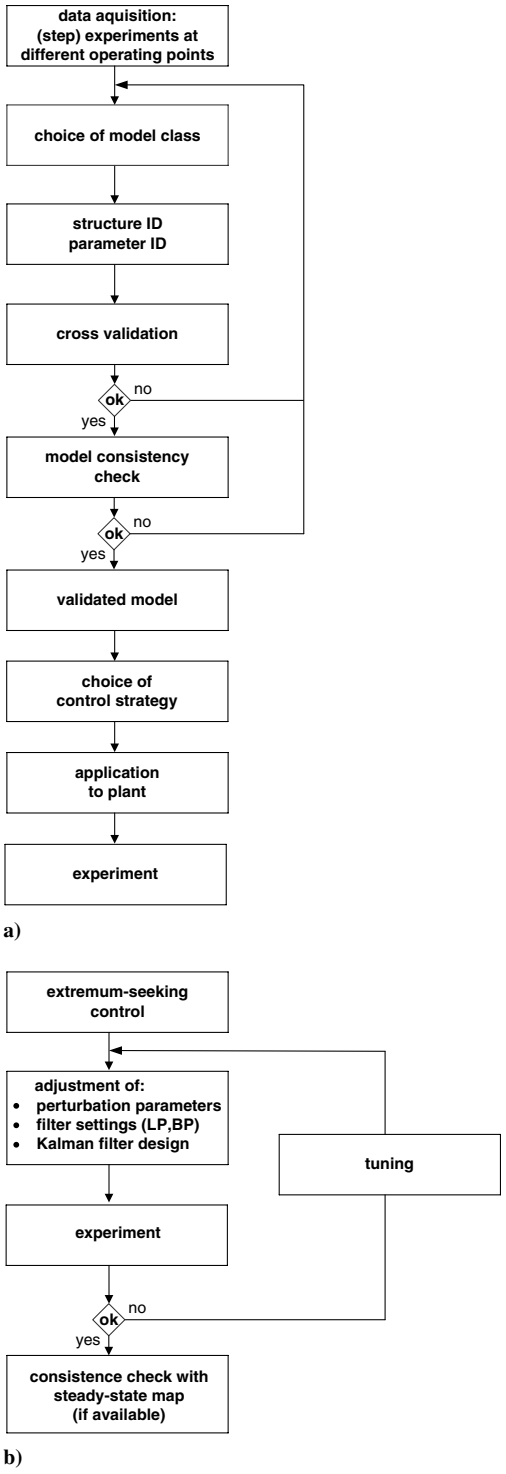

Fig. 5 Simplified work process of a) model-based control and b) proposed alternative adaptive control.

This output perturbation is analyzed in order to detect the slope of the input–output map, which is used for gradient-based optimization. To do this, the mean value y_s is removed first by a second-order bandpass (BP) filter,

$$G_{BP}(j\omega) = \frac{j\omega_2}{(j\omega + \omega_1)(j\omega + \omega_2)} \tag{6}$$

with the lower and upper cutoff frequencies ω_1 and ω_2, respectively. The output of the BP filter then reads

$$y_{BP}(t) \approx |G_{BP}(j\omega_{sin})|af'\sin(\omega_{sin}t + \varphi_{BP}) \tag{7}$$

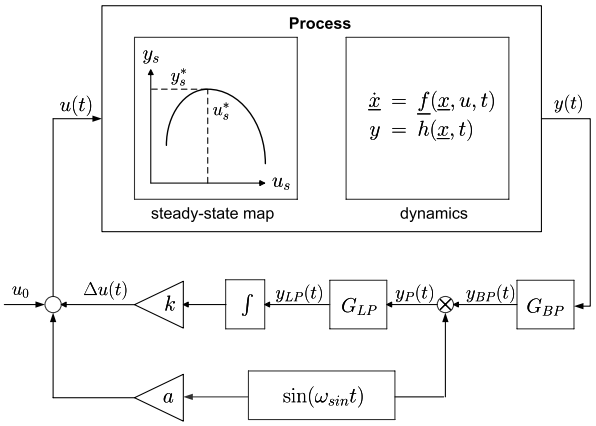

Fig. 6 Block diagram of closed-loop extremum-seeking control. The BP and LP blocks represent bandpass and low-pass filters, respectively.

The product $y_P(t)$ of this filtered output and the zero-mean sine signal $\sin(\omega_{\sin}t)$ indicates the slope of the unknown map $y_s = f(u_s)$:

$$\begin{aligned} y_P(t) &= \sin(\omega_{\sin}t)(|G_{\mathrm{BP}}(j\omega_{\sin})|af' \sin(\omega_{\sin}t + \varphi_{\mathrm{BP}})) \\ &= |G_{\mathrm{BP}}(j\omega_{\sin})|af'(\sin^2(\omega_{\sin}t)\cos(\varphi_{\mathrm{BP}}) \\ &\quad + \sin(\omega_{\sin}t)\cos(\omega_{\sin}t)\sin(\varphi_{\mathrm{BP}})) \end{aligned} \tag{8}$$

This product leads to a nonzero mean signal obtained with a low-pass (LP) filter (cf. Fig. 6), as long as the maximum is not reached. If the plant is initially to the left of the maximum, the input and output perturbations are in phase, and hence the product is positive. Accordingly, an antiphase relation that gives a negative product is an indication that the plant lies to the right of the maximum (cf. Fig. 7).

To see this, approximate the output $y_{\mathrm{LP}}(t)$ of the LP filter by an average calculated over one period $T = 2\pi/\omega_{\sin}$, i.e.,

$$\begin{aligned} y_{\mathrm{LP}}(t) &\approx \frac{1}{T}\int_0^T y_P(t)\,\mathrm{d}t = \frac{1}{T}|G_{\mathrm{BP}}(j\omega_{\sin})|af'\frac{T}{2}\cos(\varphi_{\mathrm{BP}}) \\ &= \frac{af'}{2}\Re\{G_{\mathrm{BP}}(j\omega_{\sin})\} \end{aligned} \tag{9}$$

with $\Re$ indicating the real part of a complex number. With this information an additional term $\Delta u(t)$, added to $u_0 + a\sin(\omega_{\sin}t)$, is calculated by time integration and multiplication by k [see Eq. (4) and Fig. 6]. As long as the output of the LP filter is positive, i.e., the system is on the left side of the maximum, a steadily increasing control input u is obtained, and vice versa for a negative output of the LP filter. The adaptation of u converges to $u = u^*$.

Next, extremum-seeking is extended to the general case. The assumption of an existing distinct extremum in the steady-state map is dropped, as flow phenomena are often characterized by a plateau-type behavior (cf. Fig. 4). The separated flow over turbomachinery blades is influenced by active flow control in such a way that it reattaches again. Once the flow is completely attached, a further increase of the control input will result in neither a further increase nor decrease of the lift. Starting left of the plateau the described extremum-seeking controller will function correctly in that situation. However, when the value of the control input is so large that the corresponding value of the output variable is already on top of the plateau, the actuation amplitude will not be minimized. In this situation no more gradient information is detectable for the controller. As a consequence, a waste of control energy results. For example, this situation may occur when the plateau-type map is shifted to the left due to changed operating conditions.

Therefore, an extension of the extremum-seeking scheme is necessary. Slope-seeking control [12] (see Fig. 8) provides the capability of driving the plant output to a value that corresponds to a set reference slope of the steady-state input–output map:

$$f'_{\mathrm{ref}} = \left.\frac{\partial y_s}{\partial u_s}\right|_{\mathrm{ref}} \tag{10}$$

According to Eq. (1), a negative reference value

$$r(f'_{\mathrm{ref}}) = -\frac{af'_{\mathrm{ref}}}{2}\Re\{G_{\mathrm{BP}}(j\omega_{\sin})\} \tag{11}$$

as a function of f'_{ref} is added to the actually detected slope, and thereby the apparent extremum is shifted. Setting this reference value to zero, extremum-seeking becomes a special case of slope-seeking control.

The extremum-seeking scheme is an adaptive closed-loop type of control and guarantees closed-loop stability if designed properly [12]. The speed of convergence is determined by the choice of certain design parameters.

For the results presented here we set $\omega_1 = \omega_2 = \omega_{\sin}$ because this setting avoids a phase shift ϕ_{BP}. Moreover, the LP filter is not necessary, but it is helpful in filtering out the perturbation signal after the multiplication of y_{BP} with $\sin(\omega_{\sin}t)$. The cutoff frequency of the LP filter is chosen to be $\omega_{\mathrm{LP}} = 0.1\omega_{\sin}$. Furthermore, the adaption gain k is chosen as a small value: $k = 100$ here.

B. Extended Kalman Filter to Speed Up Gradient Estimation

To increase the bandwidth, an extended Kalman filter [22] is proposed to estimate the actual gradient of the steady-state map. The basic idea of this approach is illustrated in the following.

In the classical extremum-seeking approach it is assumed that the input perturbation frequency is slower than the slowest dynamics of the process. Hence, the static input–output map reflects the behavior of the output $y(t)$. For small-enough input amplitudes a, the amplitude of the output perturbation should be af', as already explained in Sec. III.A. Hence, the output signal approximately consists of a constant value and the perturbation part added [see Eq. (5)],

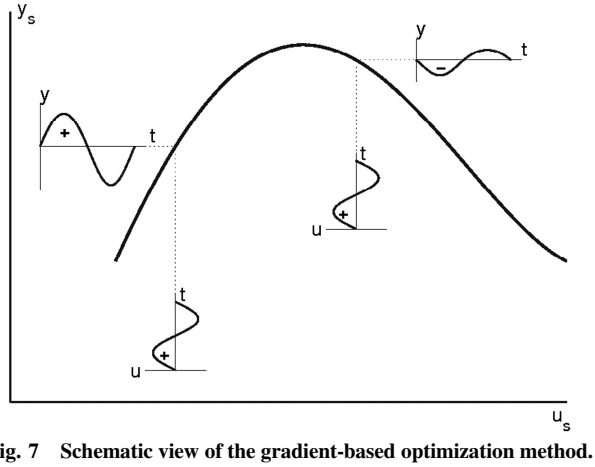

Fig. 7 Schematic view of the gradient-based optimization method.

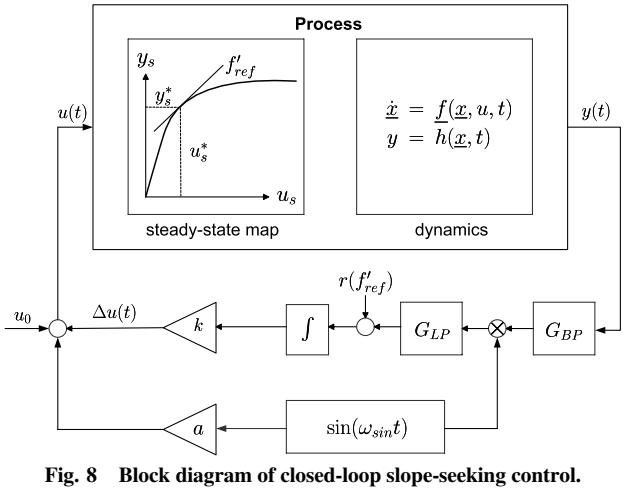

Fig. 8 Block diagram of closed-loop slope-seeking control.

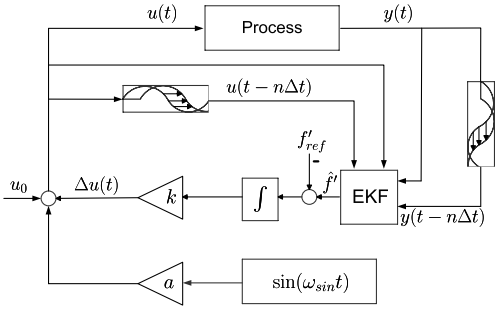

Fig. 9 Block diagram of the closed-loop slope-seeking control with an extended Kalman filter replacing the LP and BP of Fig. 6.

$$y(t) \approx y_s + af' \sin(\omega_{\sin} t) \tag{12}$$

with Eq. (4),

$$y(t) \approx \underbrace{y_s - f' u_0 - f' \Delta u(t)}_{x_1} + \underbrace{f'}_{x_2} u(t) = x_1 + u(t) x_2 \tag{13}$$

only two slowly changing parameters x_1 and x_2 can be defined. These parameters are interpreted as states that can be estimated with an extended Kalman filter. To do so, a dynamical model describing the time evolution of the parameters is necessary. The most simple model assumes constant parameter values, but only in the mean. If $\underline{x} = (x_1, x_2)^T$, a stochastic model in discrete time reads

$$\underline{x}(t_{k+1}) = \begin{bmatrix} 1 & 0 \\ 0 & 1 \end{bmatrix} \underline{x}(t_k) + \underline{w}_k \tag{14}$$

where $\underline{w}_k$ accounts for a discrete-time noise to model possible changes of $\underline{x}$. This is a classical approach to estimate constant values with a Kalman filter [22]. With Eq. (14) and (13) used as a measurement equation, observability of x_1 and x_2 is not given. To make observability possible, a second pair of time-shifted input–output values $(u(t_k - n\Delta t), y(t_k - n\Delta t)) = (u(t_{k-n}), y(t_{k-n}))$ has to be introduced. With $y_1(t_k) = y(t_k)$ and $y_2(t_k) = y(t_{k-n})$, respectively, $u_1 = u(t_k)$ and $u_2 = u(t_{k-n})$, the measurement equation reads

$$\underline{y}(t_k) = \begin{pmatrix} y_1(t_k) \\ y_2(t_k) \end{pmatrix} = \begin{bmatrix} 1 & u_1 \\ 1 & u_2 \end{bmatrix} \underline{x}(t_k) + \underline{v}_k \tag{15}$$

with $\underline{v}_k$ denoting white noise of the measurement. Now, an extended Kalman filter can be used for real-time estimation of the states. The modification of the slope-seeking control by inclusion of this model-based sensor is shown in the block diagram in Fig. 9. Since the extended Kalman filter estimates the slope $\hat{f}' = \hat{x}_2$, the reference slope f'_{ref} can be subtracted directly from $\hat{f}'$.

IV. Results

A. Closed-Loop Control at a Fixed Operating Point

The following closed-loop control experiments are conducted with a fixed throttle position, as mentioned before. Figure 10a presents the results obtained with a classical extremum-seeking controller.

In the beginning, the flowfield is stalled, which is indicated by the low value of the pressure coefficient $\psi = 0.34$. At $t = 4$ s control is switched on. The injected mass flow grows by continuously increasing the duty cycle of the valves. At $t = 18$ s the flow coefficient exceeds $\psi = 0.46$. As this value corresponds to the maximally achievable value of the pressure coefficient, we assume that the flow has reattached. We use the time needed to reach this value as an indication of the speed of the controller. The adjusted parameters for the extremum-seeking controller (ESC), the slope-seeking controller (SSC), and the slope-seeking controller with an extended Kalman filter (SSC with EKF) are given in Table 2 and have been chosen such that a maximal speed is obtained while maintaining the robustness of the approach.

After the flow reattaches, the increase of the actuation amplitude is reduced by the controller. However, a very small ascent remains, whereas the pressure coefficient remains constant. The control algorithm still detects a weakly positive gradient above the reattachment point (cf. Fig. 4).

Better suited for systems characterized by a plateau-type behavior is the slope-seeking controller (see Sec. III). The results obtained are presented in Fig. 10b. The controller is again switched on at $t = 4$ s. The flow reattaches at about 8 s later without an overshooting response. Compared with the classical approach, this indicates a reduction of about 40% in reattachment time. As a very flat gradient is still detectable at the reattachment point, as discussed above, a reference slope close to zero is chosen, with $f'_{\text{ref}} = 0.002$. Now, a sudden shift in the operating point can be detected by the slope-seeking controller with resulting lower values of m_{in}. An adequate choice of the reference slope value is important. As indicated in Fig. 5, this can be done after the implementation of the controller.

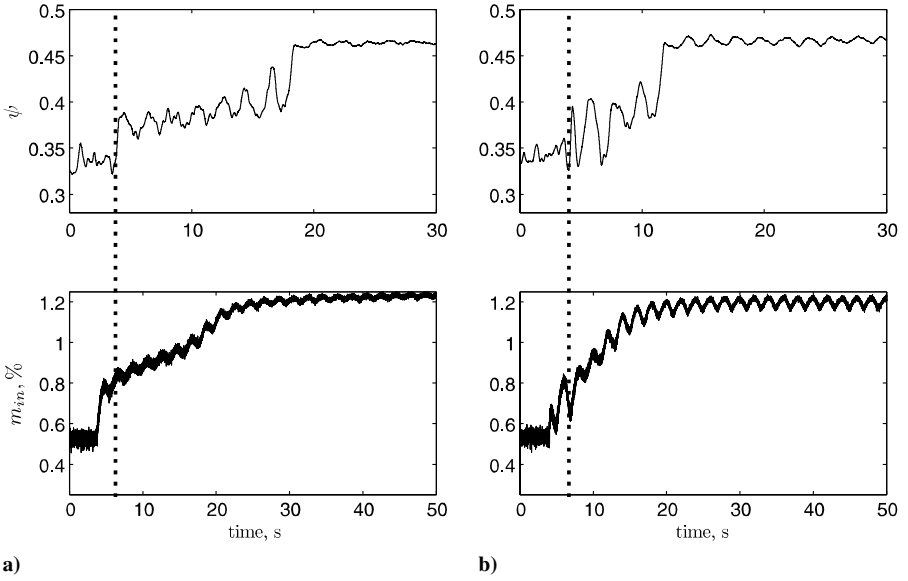

Fig. 10 Closed-loop experiment with a) extremum-seeking controller and b) slope-seeking controller. Actuation starts at the time indicated by the dashed black line.

Table 2 Adjusted controller parameters

Parameter	SSC with EKF	SSC	ESC
Sampling frequency, Hz	2000	1000	1000
Perturbation frequency $\omega_{\sin}$, Hz	2.0	0.4	0.5
Perturbation amplitude a[a], %	7	10	5
Starting control input u_0[a], %	20	20	20
Cutoff frequency of LP, Hz	——	0.04	0.05
Cutoff frequency of BP, Hz	——	0.4	0.5
Amplification gain k	10,000	80	100
Reference slope f'_{ref}	0.002	0.002	——
Delay, time samples	125	——	——
Initial covariance matrix of estimation error P_0	$\begin{pmatrix} 0.01 & 0 \\ 0 & 10 \end{pmatrix}$	——	——
Covariance matrix of the measurement noise R	$\begin{pmatrix} 0.0012 & 0 \\ 0 & 0.0012 \end{pmatrix}$	——	——
Covariance matrix of process noise Q	$\begin{pmatrix} 0.01 & 0 \\ 0 & 10 \end{pmatrix}$	——	——

[a]Values refer to the duty cycle of the valves.

Here, the chosen perturbation frequency $\omega_{\sin}$ is lower than in the classical approach, whereas the chosen perturbation amplitude a is higher. As a result, the output fluctuations are larger than those of the classical method. The complete set of controller parameters is given in Table 2.

To speed up the control performance even more, the approach of gradient estimation via a Kalman filter is tested next. The corresponding results are presented in Fig. 11. Again, the controller is switched on at $t = 4$ s. For this method a higher perturbation frequency can be chosen, leading to faster results, whereas the amplitudes of input and output signals have a smaller amplitude compared with the results shown in Fig. 10. Moreover, the controller shows a overshooting behavior, but this time it is capable of driving the system out of stall in only 1.5 s. This indicates an improvement in reattachment time of nearly a whole order of magnitude, compared with the classical approach. At $t = 19$ s the controller is switched off again, and the experiment is repeated at $t = 26$ s to confirm the first result.

The appropriate choice of the delay time between the time-shifted input–output pairs of the control input $u(t)$ [respectively, the measurement $y(t)$] is crucial, as explained in Sec. III.B. In this case, a delay of 125 samples is chosen with a sampling time of $\Delta t = 0.0005$ s. As the gradient estimation by the EKF is quite fast, it is possible to raise the perturbation frequency up to $\omega_{\sin} = 2$ Hz. With these parameters, control gets significantly faster. Higher values cannot be used, since the system is then no longer able to follow the excitation at all. As the slopes detected by the EKF are very small, a high amplification of $k = 10,000$ has to be chosen. A list of parameters is given in Table 2.

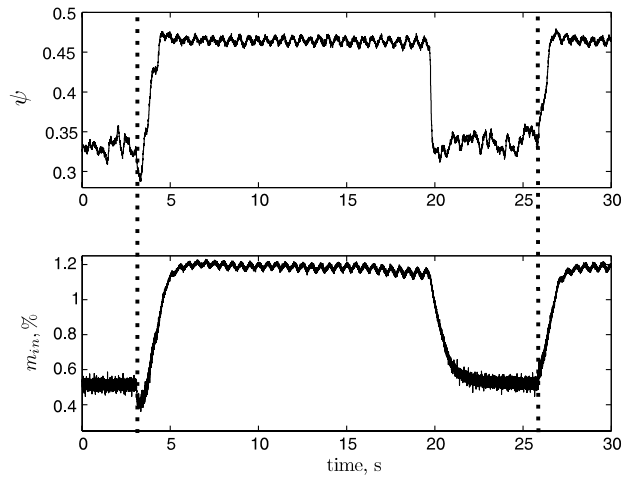

Fig. 11 Same as in Fig. 10 with gradient estimation via an EKF.

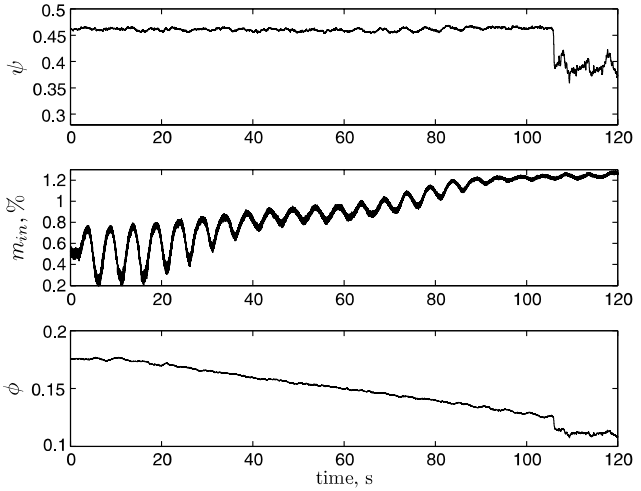

Fig. 12 Slope-seeking control with changing operating point.

B. Closed-Loop Control with Shifting Operating Points

Any controller proposed has to prove robustness to become an interesting candidate for practical application in a complex technical apparatus such as an aircraft propulsion system. The capability of reacting fast enough to changes in the environment and the capability of suppressing disturbances are indispensable. Therefore, the control algorithm proposed above is tested under quickly changing operating conditions. This is realized by bringing large-amplitude disturbances to the system by moving the throttle to lower flow coefficients. The initial operating point is chosen just before the stall point of the unactuated flow (cf. Fig. 3). The results obtained with the slope-seeking controller without EKF can be seen in Fig. 12. In the lower diagram the shift of the operating point from $\phi = 0.175$ to 0.11 is indicated. The further the operating point is shifted to lower flow coefficients the more injected mass flow is necessary to avoid flow separation. The controller reacts to the changing operating point by increasing the mass flow. Hence, the pressure coefficient remains at a constant value of about $\psi = 0.46$ and the flow can be held attached. Regarding the behavior of the injected mass flow in the middle diagram of Fig. 12, it has to be noted that the apparent adaptation of the perturbation amplitude is caused by the nonlinear relation between the adjusted duty cycle and the output mass flow. The flow remains attached until the throttle passes a value of $\phi = 0.125$, then the pressure coefficient drops. At this operating point, even a maximal actuation amplitude is not capable of avoiding stall.

Next, the approach with a Kalman filter extension for gradient estimation is tested with respect to robustness. As in the experiments shown before, the smaller fluctuations of the input variable with a

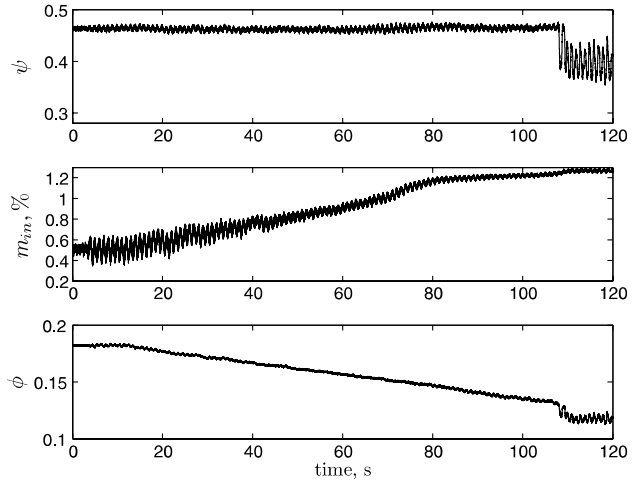

Fig. 13 Same as Fig. 12 but with gradient estimation via an EKF.

faster chosen frequency can be seen (cf. Fig. 13). By continuously opening the valves, stall can be avoided until a flow coefficient of $\phi = 0.125$ is reached.

Before flow separation, both presented controllers are able to increase the fan pressure rise by 25%, compared with the unactuated case.

V. Conclusions

The present work shows an application of extremum-seeking control methods with extensions for an axial fan to enlarge the usable range of the fan characteristic and to avoid stalled blade flow conditions. Regarding the complexity of the setup, an adaptive model-free control strategy is preferred over the classical model-based control. With model-free control, time-consuming identification processes can be avoided and, in addition, the applicability of the proposed control approach is rather simple. An important goal of the control proposed is to expedite the reattachment time of the separated flow.

Beginning with a classical extremum-seeking controller, the reattachment time amounts to 14 s. This approach is rather slow and runs the risk of wasting control energy. A slope-seeking extension reduces the time to flow reattachment down to 8 s and keeps the actuation energy, i.e., the injected mass flow to a constant minimal value. A further significant reduction of the reattachment time to 1.5 s is achieved by implementation of an extended Kalman filter for gradient estimation.

The robustness of the proposed controllers is demonstrated by shifting the operating point continuously without driving the system into stall. An increase of 25% of the fan pressure rise can be reached by active flow control.

A further improvement of the overall fan performance seems possible if the axial fan rotor and the downstream stator row are influenced in a synchronized fashion. For that reason, a stator cascade is investigated in a parallel study [25]. The common goal of both studies is to exploit the individual results and apply active flow control to rotor and stator of a complete fan stage.

Another possibility to enhance the results obtained so far is to work with higher actuation frequencies. This is the subject of ongoing research within the present project. In particular, fast control valves that can be operated in the rotor blade-passing frequency range are likely to have a significant impact on the flow physics of the blade tip region, as a synchronization of the actuation and the position of a blade seems possible.

Acknowledgments

This work is funded by the Deutsche Forschungsgemeinschaft (DFG) and by the industrial partner Rolls-Royce Deutschland as a part of the transfer project "DFG-TFB Rolls-Royce: Smart Active Control for Turbomachinery Blades."

References

[1] Lord, W. K., MacMartin, D. G., and Tillmann, G., "Flow Control Opportunities in Gas Turbine Engines," AIAA Flow Control Conference, AIAA Paper 2000-2234, Denver, CO, June 2000.

[2] Schulz, J., Garwon, M., Satriadarma, B., King, R., Möser, M., and Neise, W., "Adaptive and Robust Control for the Reduction of Tonal Noise Components of Axial Turbomachinery with Flow Control," *Proceedings of DAGA 2004*, Strasbourg, France, March 2004.

[3] Neuhaus, L., and Neise, W., "Active Flow Control to Improve the Aerodynamic and Acoustic Performance of Axial Turbomachines," AIAA Flow Control Conference, AIAA Paper 2002-2948, St. Louis, MO, June 2002.

[4] Nelson, E. B., Paduano, J. D., and Epstein, A. H., "Active Stabilization of Surge in an Axicentrifugal Turboshaft Engine," *Journal of Turbomachinery*, Vol. 122, No. 3, 2000, pp. 485–493. doi:10.1115/1.1304915

[5] Weigl, H. J., and Paduano, J. D., "Application of H_∞-Control with Eigenvalue Perturbations to Stabilize a Transonic Compressor," *Proceedings of the 1997 Conference on Control Applications*, Hartford, CT, June 1997.

[6] Eveker, K. M., Gysling, D. L., Nett, C. N., and Sharma, O. P., "Integrated Control of Rotating Stall and Surge in High-Speed Multistage Compression Systems," *Journal of Turbomachinery*, Vol. 120, No. 3, 1998, pp. 440–445. doi:10.1115/1.2841735

[7] Walsh, P. P., and Fletcher, P., *Gas Turbine Performance*, 2nd ed., Blackwell Science, Boston, MA, 2000, Chap. 8.

[8] Tavakoli, S., Griffin, I., and Fleming, P., "An Overview of Compressor Instabilities: Basic Concepts and Control," *Proceedings of the 16th IFAC International Symposium on Automatic Control in Aerospace*, St. Petersburg, Russia, June 2004.

[9] Kameier, F., and Neise, W., "Experimental Study of Tip Clearance Losses and Noise in Axial Turbomachines and Their Reduction," *Journal of Turbomachinery*, Vol. 119, No. 3, 1997, pp. 460–471. doi:10.1115/1.2841145

[10] Pack, L., Yao, C. S., and Seifert, A., "Active Control of Separation from the Flap of a Supercritical Airfoil," *AIAA Journal*, Vol. 44, No. 1, 2006, pp. 34–41. doi:10.2514/1.12225

[11] Dorf, C. D., and Bishop, R. H., *Modern Control Systems*, 9th ed., Prentice–Hall, Upper Saddle River, NJ, 2000, Chap. 4.1.

[12] Ariyur, K., and Krstic, M., *Real—Time Optimization by Extremum-Seeking Control*, 1st ed., Wiley, Hoboken, NJ, 2003, Chaps. 4, 6.

[13] Krstic, M., and Wang, H. H., "Stability of Extremum-Seeking Feedback for General Nonlinear Dynamic Systems", *Automatica*, Vol. 36, No. 4, 2000, pp. 595–601. doi:10.1016/S0005-1098(99)00183-1

[14] Becker, R., King, R., Petz, R., and Nitsche, W., "Adaptive Closed-Loop Separation Control on a High-Lift Configuration Using Extremum Seeking," *AIAA Journal*, Vol. 45, No. 6, 2007, pp. 1382–1392. doi:10.2514/1.24941

[15] Inoue, M., and Kuroumaru, M., "Structure of Tip Clearance Flow in an Isolated Axial Compressor Rotor," *Journal of Turbomachinery*, Vol. 111, No. 3, 1989, pp. 250–256. doi:10.1115/1.3262263

[16] Weigl, H. J., Paduano, J. D., Fréchette, L. G., Epstein, A. H., Greitzer, E. M., Bright, M. M., and Strazisar, A. J., "Active Stabilization of Rotating Stall and Surge in a Transonic Single Stage Axial Compressor," *Journal of Turbomachinery*, Vol. 120, No. 4, 1998, pp. 625–636. doi:10.1115/1.2841772

[17] Paduano, J. D., Epstein, A. H., Valavani, L., Longley, J. P., Greitzer, E. M., and Guenette, G. R., "Active Control of Rotating Stall in a Low-Speed Axial Compressor," *Journal of Turbomachinery*, Vol. 115, No. 1, 1993, pp. 48–56. doi:10.1115/1.2929217

[18] Nelson, E. B., Paduano, J. D., and Epstein, A. H., "Active Stabilization of Surge in an Axicentrifugal Turboshaft Engine," *Journal of Turbomachinery*, Vol. 122, No. 3, 2000, pp. 485–493. doi:10.1115/1.1304915

[19] Lemke, O., Becker, R., Feuerbach, G., Neise, W., King, R., and Möser, M., "Active Blade Tone Control in Axial Turbomachines by Flow Induced Secondary Sources in the Blade Tip Regime," *Notes on Numerical Fluid Mechanics and Multidisciplinary Designs*, 1st ed., Vol. 95, Springer, Berlin, 2007, pp. 391–407.

[20] Wang, H. H., Yeung, S., and Krstic, M., "Experimental Application of Extremum-Seeking on an Axial-Flow Compressor," *Proceedings of the American Control Conference 1998*, IEEE, Piscataway, NJ, June 1998, pp. 1989–1993.

[21] Henning, L., Becker, R., Feuerbach, G., Muminovic, R., and King, R., "Extensions of Adaptive Slope-Seeking for Active Flow Control," *Journal of Systems and Control Engineering*, Vol. 222, No. 5, 2008, pp. 309–322. doi:10.1243/09596518JSCE490

[22] Gelb, A., *Applied Optimal Estimation*, 16th ed., 2001, M.I.T. Press, Cambridge, MA, pp. 107–127.

[23] Neuhaus, L., and Neise, W., "Active Flow Control to Reduce the Tip Clearance Noise and Improve the Aerodynamic Performance of Axial Turbomachines," *Fan Noise 2nd International Symposium*, Senlis, France, May 2003.

[24] Morosanov, I. S., "Method of Extremum Control," *Automation and Remote Control*, Vol. 18, 1957, pp. 1077–1092.

[25] Hecklau, M., Wiederhold, O., Zander, V., King, R., Nitsche, W., and Swoboda, M., "Active Separation Control with Pulsed Jets in a Critically Loaded Compressor Cascade," AIAA 5th Flow Control Conference, AIAA Paper 10-4252, Chicago, June 2010.

N. Wereley
Associate Editor